Journal of
Nanoscience and Nanotechnology
Vol. 12, 4919–4927, 2012

Increasing Active Surface Area to Fabricate Ultra-Hydrophobic Surface by Using "Black Silicon" with Bosch Etching Process

Nithi Atthi[1,*], Jakrapong Supadech[1], Gaëtan Dupuy[2], On-uma Nimittrakoolchai[3], Apirak Pankiew[1], Sitthisuntorn Supothina[3], Wutthinan Jeamsaksiri[1], Charndet Hruanun[1], Amporn Poyai[1], and Claire-Helene Brachais[2]

[1] National Electronics and Computer Technology Center, 112 Thailand Science Park, Paholyothin Rd., Klong Luang, Pathumthani, 12120, Thailand
[2] Engineering School for Material Research, University of Burgundy, 9 Avenue Alain Savary, BP 47870, Dijon, 21078, France
[3] National Metal and Materials Technology Center, 114 Thailand Science Park, Paholyothin Rd., Klong Luang, Pathumthani, 12120, Thailand

Needle-shaped pillars so-called "Black silicon" (B–Si) were fabricated by etching cleaned silicon wafer with fluorine-based deep reactive ion etching plasma. The B–Si pillar with the pillar size (*a*) and spacing (*b*) of 250 nm, and height (*h*) of 6.47 μm, coated with SiO_xF_y film had water contact angle (WCA) and ethylene glycol contact angle (ECA) of 159.8° and 135.5°, respectively. After coating the pillar with trichloro(1H,1H, 2H,2H-perfluorooctyl)silane (TPFS), the WCA and ECA increased to 166.2° and 161.8°, respectively. At the optimum etching condition, the B–Si pillar with the size $a = 376$ nm, $b = 576$ nm, $h = 6.47$ μm, and the aspect ratio of 14.80 showed the WCA and ECA of 4.25° and 14.77°, respectively. After coating with the TPFS, liquid droplets ran across the sample's surface rapidly and the WCA and ECA could not be measured. Moreover, when the pillar height was increased twice, the WCA and ECA of the B–Si with and without the TPFS coating were greater than 170°, indicating excellent water-and-oil repellency and can be applied for Micro-Electro-Mechanical Systems (MEMS).

Keywords: Black Silicon, DRIE, MEMS, Superhydrophobic, Water Repellency.

RESEARCH ARTICLE

1. INTRODUCTION

In recent years, there are many techniques employed to fabricate a multi-scaled roughness so as to mimic a superhydrophobic surface similar to that of lotus leaf which has water contact angle (WCA) greater than 150°.[1–3] The superhydrophobicity is a combined effect of low surface energy material and rough surface.[4] This surface has generated wide interest due to its great potential for various applications including water-repellence,[2] anti-adhesion,[5] anti-fouling,[6] and various Micro-Electro Mechanical Systems (MEMS) such as micro-fluidic device.[5,7] The WCA on a rough surface can be calculated by Wenzel's model, which relates the surface roughness factor, *r*, and Young's contact angle, θ_y.[8] The maximum WCA on the rough surface can be obtained by maximizing *r*, or minimizing the pillar size (*a*), and the space between the pillar (*b*), and to maximize the pillar height (*h*).[9–12] Unfortunately, this optimized structure can only be fabricated by using ultra-high resolution lithographic and high selectivity reactive ion etching (RIE). To avoid using those expensive tools, the high packing factor (a/b) and high aspect ratio, A.R, (h/a) pillar can be obtained by using the "Black silicon," B–Si, nano-structure. The B–Si can be fabricated by using Fluorine-based RIE plasma (SF_6/O_2) etching process without any expensive lithography tool. The SF_6 produces the F* radicals for the chemical etching of the Si forming the volatile SiF_4. O_2 creates the O* radicals to passivate the Si surface with siliconoxyfluoride (SiO_xF_y).[13,14] In that time, native oxide and dust in the vacuum chamber will act as micro masks and block the plasma to generate the spikes coated with a thin SiO_xF_y film.[13–16] The mechanism of formation is shown in Figure 1. This research work aimed to study the effect of RIE condition on the

*Author to whom correspondence should be addressed.

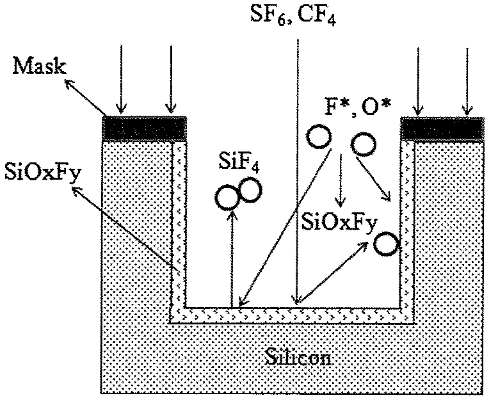

Fig. 1. Forming mechanism of black silicon during RIE process.

formation of B–Si. Water contact angle and ethylene glycol contact angle (ECA) on the B–Si nanostructure are also investigated.

2. EXPERIMENTAL DETAILS

2.1. Effect of RIE and Bosch's Process Conditions on WCA and ECA

This experiment aimed to study effects of the etch process parameters on the formation of black silicon. The etching system used in this experiment was Oxford Plasmalab 100 which has 10 adjustable parameters; (1) Etch time (sec), (2) Chamber pressure (mtorr = 0.133 Pa), (3) Valve angle (°), (4) C_4F_8 gas flow (sccm = standard cubic centimeters per minute), (5) SF_6 gas flow (sccm), (6) O_2 gas flow (sccm), (7) He cooling gas flow (sccm), (8) Radio frequency (RF) power (Watt), (9) Inductively coupled plasma (ICP) power (Watt), and (10) DC bias (volt). 6-inch silicon wafer with (100) plane was used as a substrate. The wafer was cleaned with Piranha acid solution (H_2SO_4:H_2O_2 at 4:1 %vol.) at 120 °C for 15 min, then rinsed with de-ionized water (DIW) for 10 min and blow dried with N_2. There were 4 different etching conditions. Sample S1 was etched by RIE and followed by deep reactive ion etching (DRIE) Bosch's process at 27 loops (1 loop is the combination between etching and depositing step). Sample S2 and S3 were etched by only RIE process but the RF power for S3 was greater than that in S2. Sample S4 was etched by only DRIE Bosch's process at 27 loops. This means that, SF_6 flow, O_2 flow and the chamber pressure were varied during a DRIE Bosch's etching process for S1 and S4. The ICP power and DC bias were fixed at 2,000 watts and 117 volts, respectively. The etching conditions are shown in Table I. The B–Si nano-pillars were later coated with trichloro(1*H*,1*H*, 2*H*,2*H*-perfluorooctyl)silane (TPFS) by dip coating technique and then hard baked in an electric oven at 120 °C for 60 min.

Table II. The RIE conditions from $L_{27}(3^6)$ taguchi's DOE.

Runs	(A) Etch time (sec)	(B) SF_6 flow (sccm)	(C) O_2 flow (sccm)	(D) He flow (sccm)	(E) RF power (watt)	(F) ICP power (watt)
DOE#1	10	20	20	8	15	1,500
DOE#2	10	20	20	8	45	2,000
DOE#3	10	20	20	8	75	2,500
DOE#4	10	40	60	10	15	1,500
DOE#5	10	40	60	10	45	2,000
DOE#6	10	40	60	10	75	2,500
DOE#7	10	60	100	12	15	1,500
DOE#8	10	60	100	12	45	2,000
DOE#9	10	60	100	12	75	2,500
DOE#10	15	20	60	12	15	2,000
DOE#11	15	20	60	12	45	2,500
DOE#12	15	20	60	12	75	1,500
DOE#13	15	40	100	8	15	2,000
DOE#14	15	40	100	8	45	2,500
DOE#15	15	40	100	8	75	1,500
DOE#16	15	60	20	10	15	2,000
DOE#17	15	60	20	10	45	2,500
DOE#18	15	60	20	10	75	1,500
DOE#19	20	20	100	10	15	2,500
DOE#20	20	20	100	10	45	1,500
DOE#21	20	20	100	10	75	2,000
DOE#22	20	40	20	12	15	2,500
DOE#23	20	40	20	12	45	1,500
DOE#24	20	40	20	12	75	2,000
DOE#25	20	60	60	8	15	2,500
DOE#26	20	60	60	8	45	1,500
DOE#27	20	60	60	8	75	2,000

2.2. Optimization of RIE Condition for Black Silicon Formation Using Taguchi's Design of Experiments (DOE)

In this experiment, parameters of the RIE process affecting the formation of the B–Si were studied to find the

Table I. RIE and Bosch etching conditions for B–Si formation.

Sample	Process	Chamber pressure (mTorr)	Valve angle (°)	Gas flow (sccm) C_4F_8	SF_6	O_2	He	RF power (Watt)	Process time (sec)
	RIE	23.5	35	—	20	60	10	15	15
S1	Bosch (deposit)	18.0	50	200	—	—	10	10	8
	Bosch (etch)	18.0	50	—	150	—	10	15	5
S2	RIE	23.5	35	—	20	60	10	15	15
S3	RIE	23.5	35	—	20	60	10	40	15
S4	Bosch (deposit)	13.0	50	200	—	—	10	10	8
	Bosch (etch)	13.0	50	—	33	100	10	15	5

Table III. The DRIE's condition for bosch etching process.

Process	Chamber pressure (mTorr)	Valve angle (°)	Gas flow (sccm)				RF power (Watt)	Process time (sec)
			C_4F_8	SF_6	O_2	He		
Bosch (deposit)	20.0	50	200	—	—	10	10	4
Bosch (etch)	25.0	50	—	200	—	6	15	8

optimum condition. There were 6 parameters and each parameter was varied at 3 levels, which were; (A) etching time at 10, 15, and 20 sec, (B) SF_6 gas flow at 20, 40, and 60 sccm, (C) O_2 gas flow at 20, 60, and 100 sccm, (D) He gas flow at 8, 10, and 12 sccm, (E) RF power at 15, 45, and 75 watts, and (F) ICP power at 1,500, 2,000, and 2,500 watts. The chamber pressure and valve angle were fixed at 23.5 mtorr and 35°, respectively. Based on these parameters, there was totally 3^6 or 729 experiments with Full-factorial DOE which can be reduced to only 27 experiments by using the Taguchi's DOE: L_{27} (3^6) as shown in Table II. The optimized sample with the highest WCA and ECA was further etched with the Bosch's process using the condition shown in Table III. The etching depth was varied by changing the etching loop from 15 to 30 and 45 loops.

2.3. Characterization

Physical color of each sample was captured by a digital camera. Shape of the B–Si pillar was characterized by using a scanning electron microscope (SEM). Composition of the B–Si pillar was characterized by an Auger electron spectroscopy (AES) technique (operated at 10 kV, 10 nA, Tilt 0°, Res. 1 eV/step). Surface's wetting ability before and after coating with the TPFS was evaluated by measuring water and ethylene glycol contact angles using the 190 CA ramé-hart goniometer.

3. RESULTS AND DISCUSSION

3.1. Preliminary Result of Effect of Etching Condition on Pillar Dimension and Liquid Contact Angle

Figure 2 shows SEM images of the samples prepared by using different etching condition given in Table I. It is revealed that different shape and size of the B–Si pillar was obtained from different etching conditions. The pillar height of samples S1 to S4 was 7.26 μm, 3.61 μm, 4.21 μm, and 1.15 μm, respectively, while the pillar size varied between 50 to 200 nm. AES spectrum in Figure 3(a) revealed that the sample S1 consisted of Si, C, O, and F. The fluorine radical (F*) came from by-product from etching gases (SF_6). This means the S1 sample had SiO_xF_y thin film coated on its surface. Comparing the AES spectra

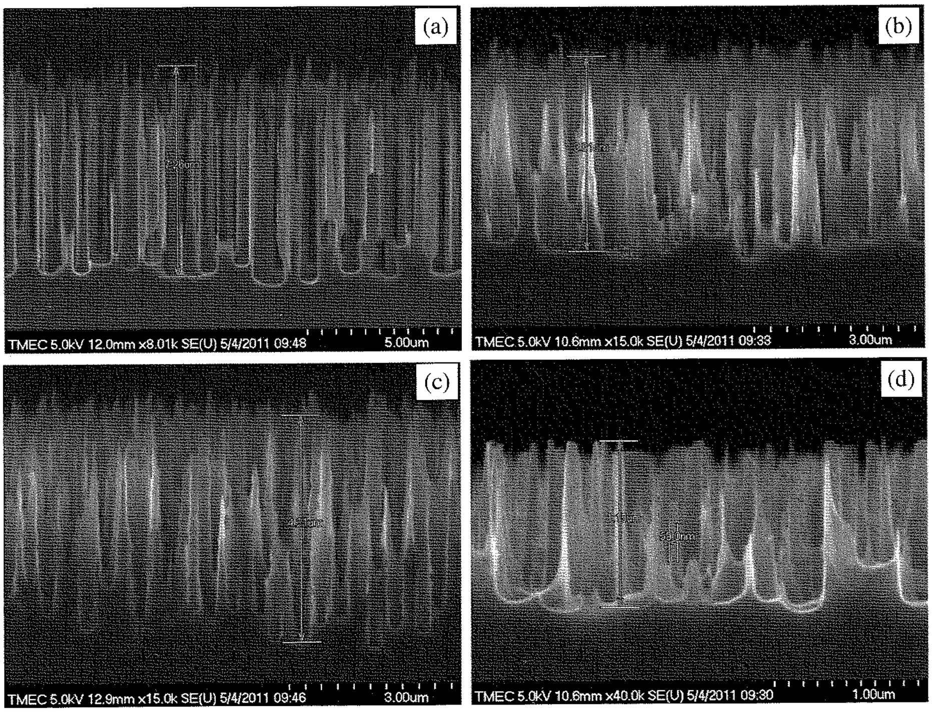

Fig. 2. SEM images of the samples fabricated from different etching condition according to Table I; (a) S1, (b) S2, (c) S3, and (d) S4.

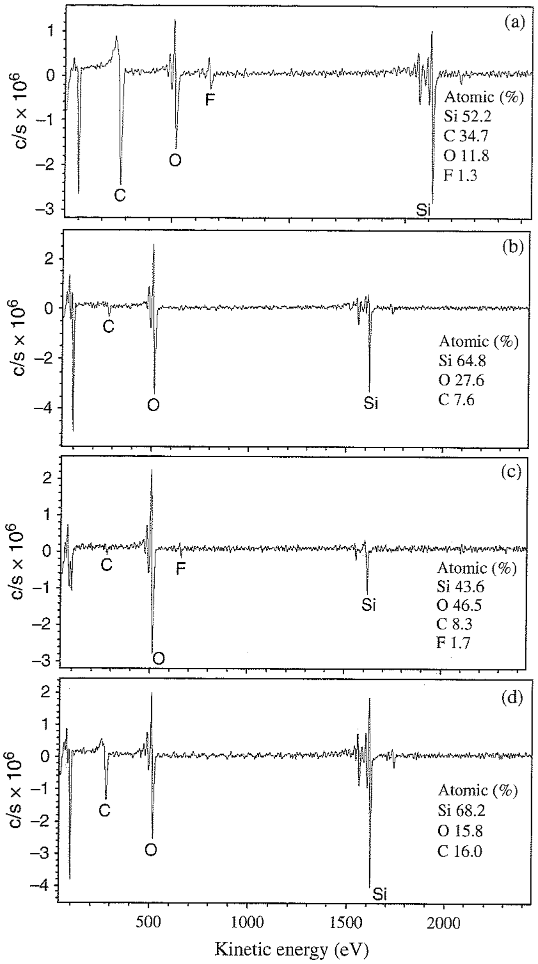

Fig. 3. Auger electron microscopy spectra of B–Si surface.

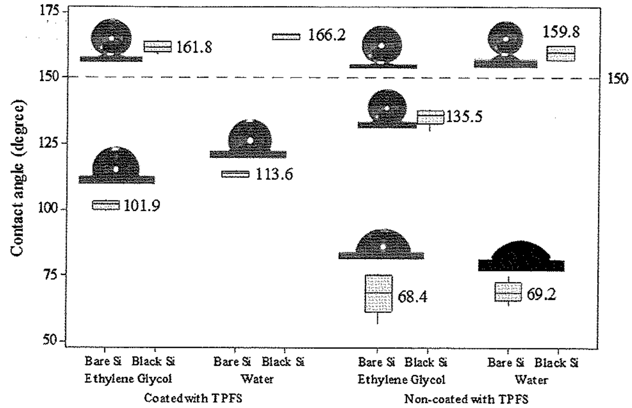

Fig. 5. Water and ethylene glycol contact angles on various surfaces.

of the samples S2 and S3 (Figs. 3(b and c), respectively), the F was found on the S3 surface but not on the S2 surface because the RF power employed to prepare the S3 was higher. Moreover, the AES spectrum of S4 (Fig. 3(d)) consisted of only Si, O, and C. F was absent because this sample was prepared by only the Bosch etching process. According to the AES analysis, the SiO_xF_y film can only be found on the B–Si pillar prepared by mixed RIE and Bosch's DRIE processes with high O_2 flow rate and high RF power.

Figures 4(a–c) shows top-view and cross-sectional view SEM images of uncoated S1 sample and Figure 4(d) shows cross-sectional image of S1 sample coated with the TPFS. The S1 sample is the uncoated B–Si had pillar structure of 250-nm wide and 6.5-μm high. After coating with the TPFS, the pillar shape and size was maintained as

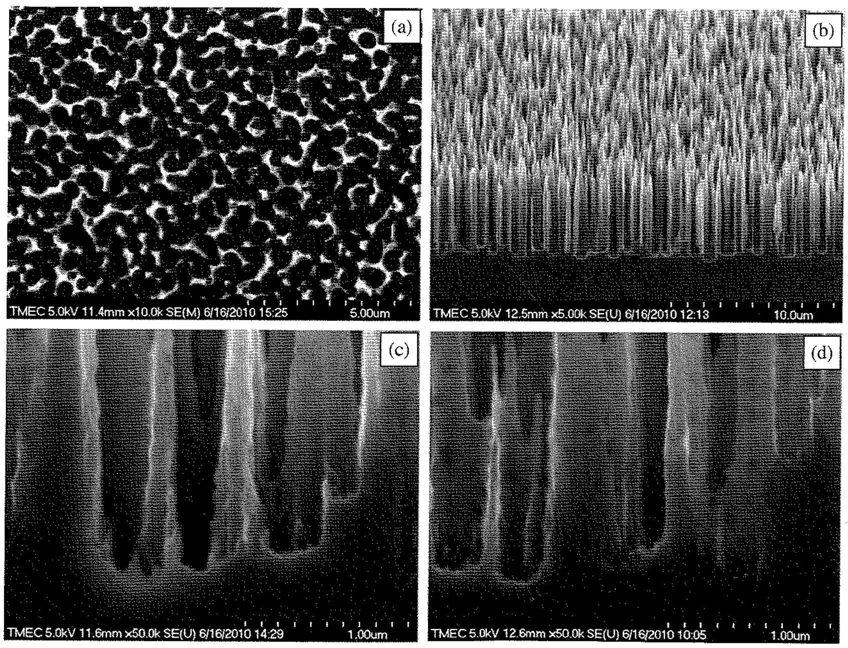

Fig. 4. SEM images of (a) top view, (b–c) cross-sectional view of B–Si, and (d) cross-sectional view of B–Si pillar coated with TPFS.

RESEARCH ARTICLE

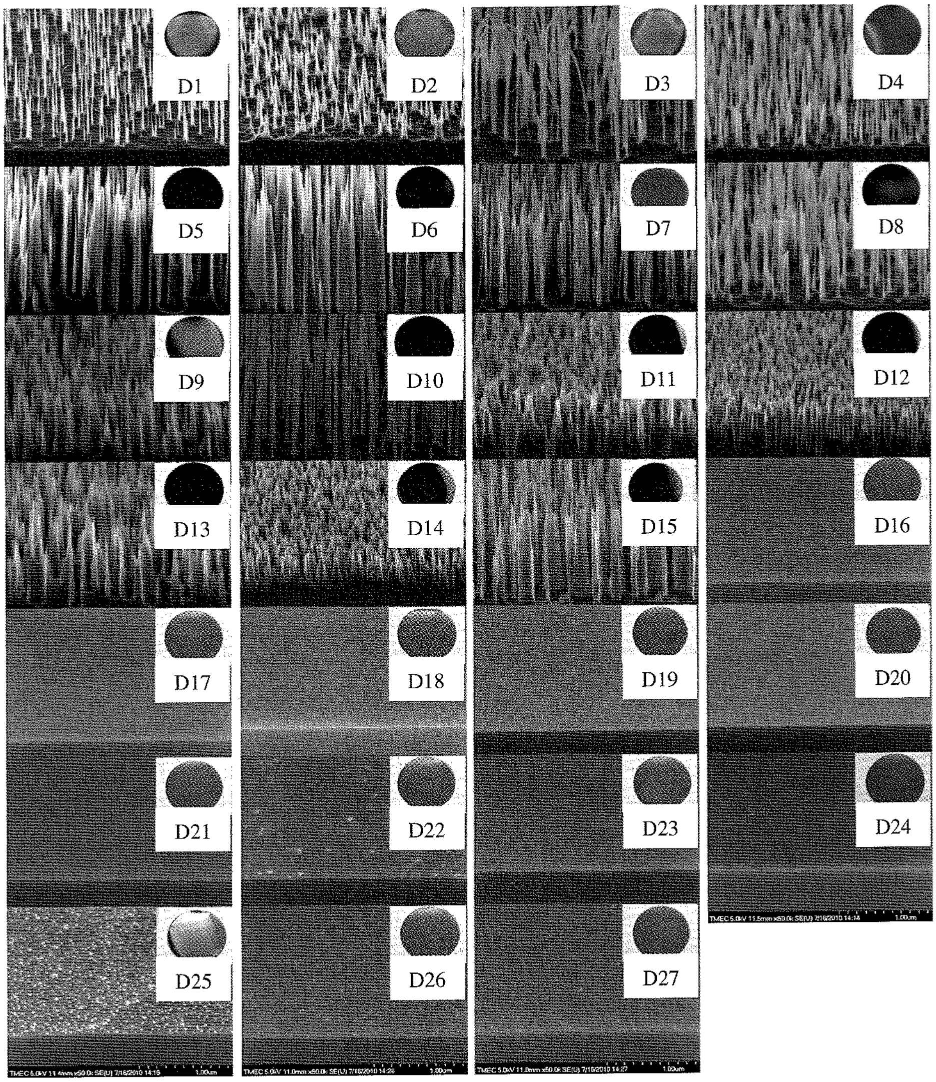

Fig. 6. Digital camera images and side-view SEM images of the wafer surface DOE#1 to DOE#27.

shown in Figure 4(d). The WCA and ECA (Fig. 5) of the uncoated B–Si surface were 159.8° and 135.5°, respectively, which were exceptionally high. Such high contact angles arose from high surface roughness of the very fine pillars. After coating with the TPFS, its WCA and ECA increased to 166.2° and 161.8°, respectively, indicating that liquid repellency can be improved by modifying the roughened surface with low-surface energy substance.

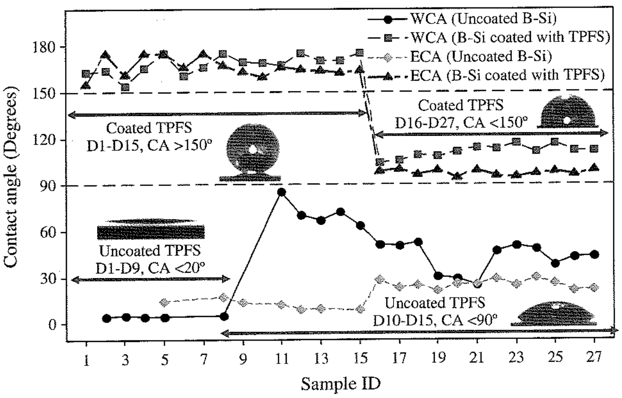

Fig. 7. WCA and ECA for the uncoated and TPFS-coated of DOE#1 to DOE#27.

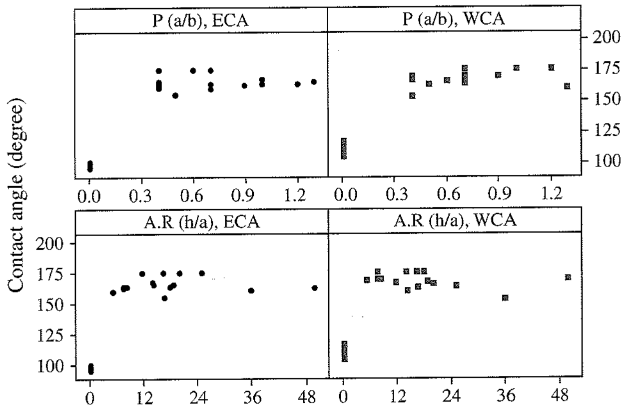

Fig. 8. Effect of aspect ratio and packing factor of B–Si pillars after coating with TPFS on the WCA and ECA.

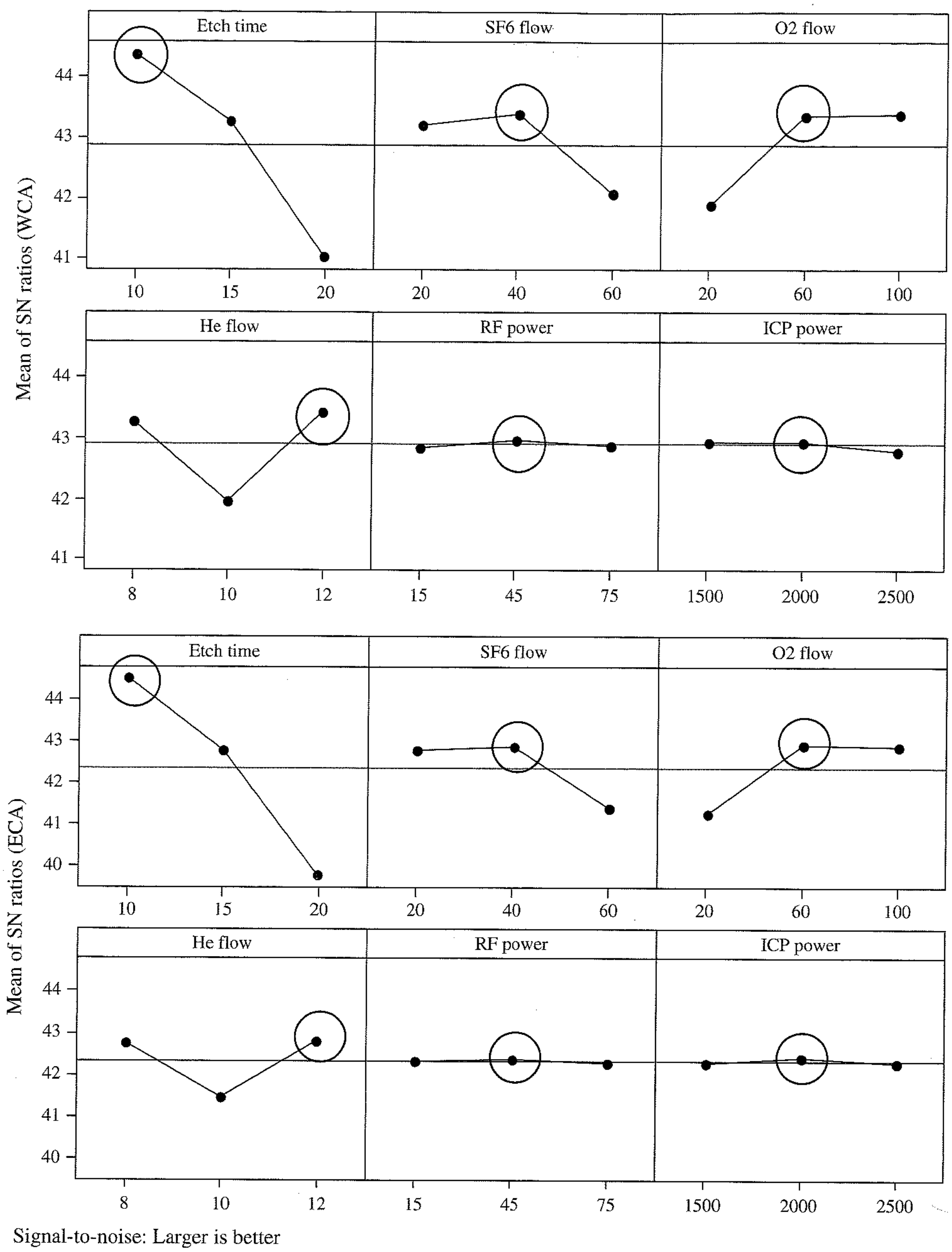

Fig. 9. Signal-to-Noise (S/N) ratio for the WCA and ECA.

3.2. Optimized Condition for Black Silicon Formation

Surface colors of the samples prepared according to the condition from the Taguchi's DOE were varied from gray to black based on the etching condition. The DOE#16 to DOE#27 had the same color as the original bare silicon. Those surfaces were very shiny, indicating their high reflectivity. Considering the DOE#1 to DOE#4, their surfaces were darker than the surfaces of the DOE#16 to DOE#27. However, the etched patterns were not uniform. The suitable conditions for black silicon formation were conditions DOE#5 to DOE#15, which gave uniform pillar patterns. 45°-tilted SEM images of the DOE#16 to DOE#27 revealed flat surfaces indicating that their surfaces have not been etched. The flat surface gave rise to high reflectance. In contrast, the B–Si pillar has been formed on the surface of DOE#1 to DOE#15. Their surface appeared black and consisted of B–Si pillar (Fig. 6) which absorbed light. Their pillar sizes, a, was in the range of 157 nm to 702 nm, the spacing between pillars, b, was in the range of 286 nm to 740 nm, and the pillar height, h, was in the range of 1.63 μm to 15.10 μm. However, the pillar dimensions were adjusted by using a packing factor, P, (a/b) and an aspect ratio, AR, (h/a). The P and AR of the DOE#1 to DOE#27 were varied from 0.4 to 1.3 and 5.2 to 50.1, respectively. The WCAs of the DOE#1 to DOE#9 were closed to 0°, indicating their ultrahydrophilic nature. The WCAs of the DOE#10 to DOE#27 were in

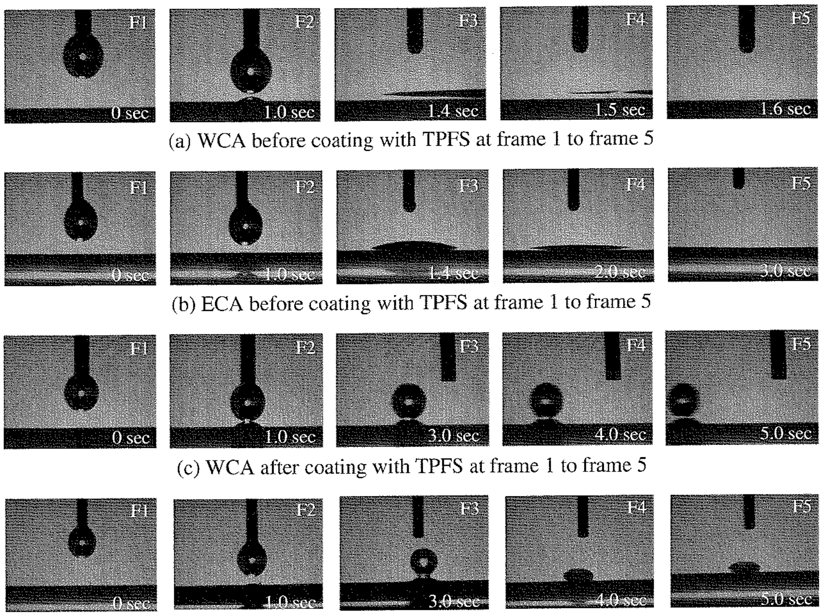

(a) WCA before coating with TPFS at frame 1 to frame 5

(b) ECA before coating with TPFS at frame 1 to frame 5

(c) WCA after coating with TPFS at frame 1 to frame 5

(d) ECA after coating with TPFS at frame 1 to frame 5

Fig. 10. Video-captured images of liquid droplets on DOE#5; (a) WCA before coating with TPFS, (b) ECA before coating with TPFS, (c) WCA after coating with TPFS, (d) ECA after coating with TPFS at frame 1, F1 (before dropping the liquid), F2 (the liquid droplet contact to the wafer surface), F3-F5 (droplet movement).

the range of 25° to 85°, indicating their hydrophilic nature. The ECAs of the DOE#1 to DOE#4 could not be measured because liquid droplets spread out instantly and the liquid droplets could not be captured by the CCD camera. The ECA of the DOE#5 to DOE#27 were also below 30°, indicating their high wetting ability. This liquid contact angle measurement indicated that surfaces of bare B–Si pillars were hydrophilic and oleophilic. After coating the B–Si pillars with TPFS, the WCAs and ECAs of the DOE#1 to DOE#15 increased to 152° or greater, indicating their superhydrophobic and superoleophobic nature. The WCAs and ECAs of the DOE#16 to DOE#27 were in the range of 100° to 120°, and 95° to 100°, respectively. Therefore, it can be concluded that the superhydrophobicity and superoleophobicity cannot be achieved on bare B–Si pillars and flat Si surface coated with the TPFS. On the other word, only the B–Si pillars coated with the TPFS can be super water- and ethylene glycol-repellent. Moreover, it was found that the ECA was smaller than the WCA in all cases as shown in Figure 7 since the ethylene glycol has lower surface tension than water.

Due to the limitation of the measurement tool, the contact angle of liquid droplets which spreaded out instantly (ultrahydrophilic) was assumed to be 5° and the contact angle of liquid droplets which ran off very fast (ultrahydrophobic) was assumed to be 175°. These assumptions were necessary to make any statistical analysis. The main effect plots (Fig. 8) revealed that when the P and AR parameters increased, the WCA and ECA of the pillars coated with the TPFS also increased. This result agrees with Wenzel's model that the smaller and taller the B–Si pillar, the higher the WCA and ECA. However, the WCA and ECA have become a constant when the P and AR parameters have greater than 0.4 and 5.2, respectively.

To find the optimized condition from the Taguchi's DOE, the smaller-the-better model was used to calculate the WCA and ECA. The signal-to-noise (S/N) ratio curve in Figure 9 shows that gas flow and etching time had

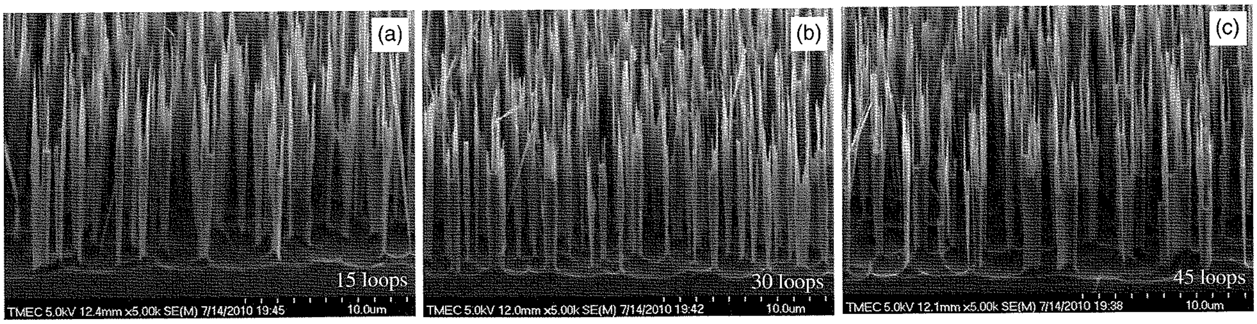

Fig. 11. Side-view SEM images of the DOE#5 B–Si pillar with (a) 15, (b) 30, and (c) 45 loops Bosch's etching process.

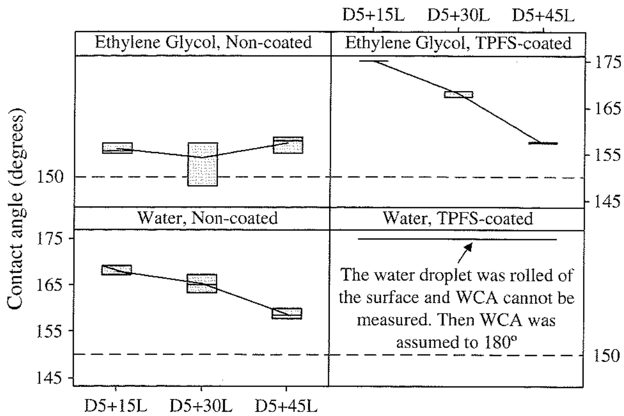

Fig. 12. WCA and ECA on the B–Si structure fabricated by varying the Bosch's etching loop.

more pronounced effect on the WCA and ECA than the RF power and ICP power. Based on the maximum signal-to-noise (S/N) ratio, the optimized RIE condition was as follow: etching time 10 sec, SF_6 gas flow 40 sccm, O_2 gas flow 60 sccm, He gas flow 12 sccm, RF power 45 watts and ICP power 2,000 watts. The predicted WCA and ECA were 191.1° and 192.3°, respectively, which were above the limitation of the contact angle (180°). Therefore, the DOE#5, which was the best condition out of all 27 experiments, was selected for experimentation of increasing a pillar height. The dimension of DOE#5 after RIE was as follow: pillar size 396 nm, pillar space 576 nm and pillar height 6.47 μm. This condition resulted in the B–Si pillar with P and AR of 0.7 and 16.3, respectively. The water and ethylene glycol droplets spread out on the sample's surface very quick, giving the WCA and ECA of 4.3° and 14.8°, respectively. After coating with the TPFS, the water and ethylene glycol droplets ran across the sample's surface, indicating its ultrahydrophobic and ultraoleophobic natures. Captured images of water and ethylene glycol droplets on the uncoated- and TPFS-coated DOE#5 are shown in Figure 10.

After continue etching the DOE#5 wafer with DRIE for 15, 30, and 45 loops by using the same condition for the Bosch's process of SN1 shown in Table I. Side-view SEM images (Fig. 11) revealed that there were no noticeable differences of the pillar shape between each etching condition. The AR of the B–Si pillar with 15, 30, and 45 etching loops increased from 14.08 by etching with only DOE#5 condition (without Bosch's etching process) to 25.15, 28.42, and 29.91, respectively. The bare B–Si pillar fabricated at 30 loops of DRIE had the WCA and ECA greater than 150° (superhydrophobic and oleophobic surface) compared to the sample fabricated by only RIE of DOE#5, which had the WCA and ECA smaller than 90° (hydrophilic and oleophilic surface). After coating with the TPFS, the WCA cannot be measured

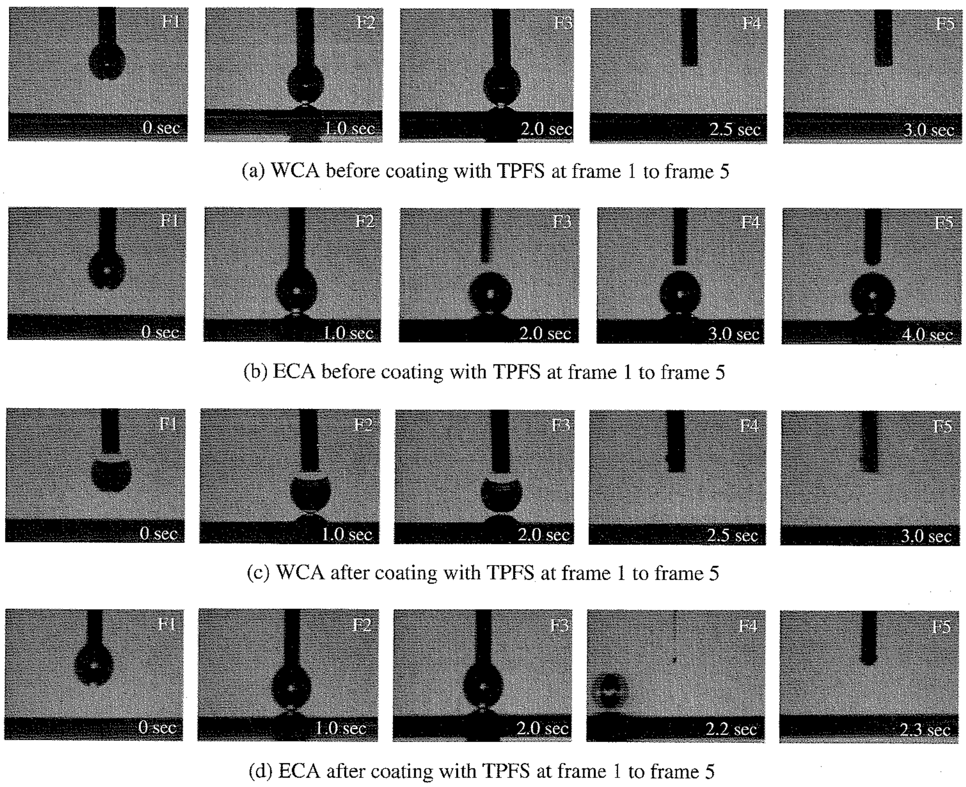

Fig. 13. Video-captured images of liquid droplets on DOE#5 with 30 loops Bosch's process; (a) WCA before coating with TPFS, (b) ECA before coating with TPFS, (c) WCA after coating with TPFS, (d) ECA after coating with TPFS at frame 1, F1 (before dropping the liquid), F2 (the liquid droplet contact to the wafer surface), F3-F5 (droplet movement).

because water droplets rolled off very easily, and the ECA increased to 175°. However, when the DRIE etching loop was increased, the WCA and ECA decreased as shown in Figure 12. The video-captured images of water and ethylene glycol droplets on the bare and TPFS-coated pillar of DOE#5 with 30 Bosch's etching loops is shown in Figure 13.

4. CONCLUSIONS

Superhydrophobic surface can be fabricated by creating very fine-scaled pillars called "Black Silicon," (B–Si). This B–Si pillar can be made without using an expensive lithography process. It is demonstrated that the B–Si can be fabricated by fluorine-based DRIE plasma (SF_6/O_2) with high O_2 flow rate. The bare B–Si pillar with an appropriate height and the SiO_xF_y film on its surface can exhibit WCA and ECA of 170.2° and 167.9°, respectively. After coating the B–Si pillar with TPFS, the water and ethylene glycol droplets ran across the surface very fast, and the WCA and ECA cannot be measured, indicating that the B–Si nanostructure can exhibit ultrahydrophobic and ultraoleophobic properties.

Acknowledgment: The authors would like to thanks to all TMEC's staffs who supported this research work. This work is also partially supported by the National Metal and Materials Technology Center, Thailand (Grant# MT-B-54-CER-07-277-I).

References and Notes

1. P. Roach, N. J. Shirtcliffe, and M. L. Newton, *Soft Matter* 4, 224 **(2008)**.
2. B. Bhushan and Y. C. Jung, *Ultramicroscopy* 107, 1033 **(2007)**.
3. M. Ma and M. H. Randal, *Curr. Opin. Colloid. In* 11, 193 **(2006)**.
4. X. M. Li, D. Reinhoudt, and M. C. Calama, *Chem. Soc. Rev.* 36, 1350 **(2007)**.
5. Z. Burton and B. Bhushan, *Nano Leters* 5, 1607 **(2005)**.
6. H. Zhang, R. Lamb, and J. Lewis, *Sci. Technol. Adv. Mat* 6, 236 **(2005)**.
7. A. J. Sceadino, H. Zhang, D. J. Cookson, R. N. Lamb, and R. De Nys, *Biofouling*. 25, 757 **(2009)**.
8. W. Li and A. Amirfazli, *J. Colloid Interf. Sci.* 28, 51 **(2007)**.
9. J. Hwang, S. H. Hong, and H. Lee, *J. Nanosci. Nanotechno.* 9, 3644 **(2009)**.
10. B. Bhushan, Y. C. Jung, and K. Koch, *Philos. T. R. Soc. A*. 367, 1631 **(2009)**.
11. W. Li, X. S. Cui, and G. P. Fang, *Langmuir* 2, 3194 **(2010)**.
12. S. Mani, P. Cassagnau, M. Bousmina, and P. Chaumont, *Macromolecules* 42, 8460 **(2009)**.
13. J. Yoo, G. Yu, and J. Yi, *Mater. Sci. Eng. B*. 333, 159 **(2009)**.
14. H. Jansen, M. de Boer, J. Burger, R. Legtenberg, and M. Elwenspoek, *Micro. Engn.* 27, 475 **(1995)**.
15. H. Jansen and M. de Boer, *Proc. IEEE, the Ninth Ann. Int. Workshop Micro Elec. Mech. Syst.*, San Diego, CA **(1996)**, pp. 250–257.
16. H. Jansen, M. de Boer, H. Wensink, B. Kloeck, and M. Elwenspoek, *Micro. Engn. J.* 32, 769 **(2002)**.

Received: 1 December 2010. Accepted: 1 May 2011.